

27-Hydroxycholesterol Enhances Secretion of Extracellular Vesicles by ROS-Induced Dysregulation of Lysosomes

Anasuya Das Gupta,¹ Jaena Park,^{2,3} Janet E. Sorrells,^{2,3} Hannah Kim,¹
Natalia Krawczynska,^{1,3} Dhanya Pradeep,¹ Yu Wang,¹ Hashni Epa Vidana Gamage,¹
Adam T. Nelczyk,¹ Stephen A. Boppart,^{2,3,4,5,6,7,8} Marni D. Boppart,^{3,5,9}
and Erik R. Nelson^{1,3,10,11,8}

¹Department of Molecular and Integrative Physiology, University of Illinois at Urbana-Champaign, Urbana, IL 61801, USA

²Department of Bioengineering, University of Illinois Urbana-Champaign, Urbana, IL 61801, USA

³Beckman Institute for Advanced Science and Technology, University of Illinois at Urbana-Champaign, Urbana, IL 61801, USA

⁴Department of Electrical and Computer Engineering, University of Illinois Urbana-Champaign, Urbana, IL 61801, USA

⁵Carle Illinois College of Medicine, University of Illinois Urbana-Champaign, Urbana, IL 61801, USA

⁶Interdisciplinary Health Sciences Institute, University of Illinois Urbana-Champaign, Urbana, IL 61801, USA

⁷NIH/NIBIB Center for Label-free Imaging and Multi-scale Biophotonics (CLIMB), University of Illinois Urbana-Champaign, Urbana, IL 61801, USA

⁸Cancer Center at Illinois, University of Illinois Urbana-Champaign, Urbana, IL 61801, USA

⁹Department of Kinesiology and Community Health, University of Illinois Urbana-Champaign, Urbana, IL 61801, USA

¹⁰Carl R. Woese Institute for Genomic Biology- Anticancer Discovery from Pets to People, University of Illinois at Urbana-Champaign, Urbana, IL 61801, USA

¹¹Division of Nutritional Sciences, University of Illinois Urbana-Champaign, University of Illinois at Urbana-Champaign, Urbana, IL 61801, USA

Correspondence: Erik R. Nelson, PhD, Department of Molecular and Integrative Physiology, University of Illinois at Urbana-Champaign, 524 Burrill Hall [MC-114], 407 S. Goodwin Ave., Urbana, IL 61801, USA. Email: enels@illinois.edu.

Abstract

Extracellular vesicles (EVs) serve as crucial mediators of cell-to-cell communication in normal physiology as well as in diseased states; they have been largely studied in regard to their role in cancer progression. However, the mechanisms by which their biogenesis and secretion are regulated by metabolic or endocrine factors remain unknown. Here, we delineate a mechanism by which EV secretion is regulated by a cholesterol metabolite, 27-hydroxycholesterol (27HC), where treatment of myeloid immune cells (RAW 264.7 and J774A.1) with 27HC impairs lysosomal homeostasis, leading to shunting of multivesicular bodies (MVBs) away from lysosomal degradation, toward secretion as EVs. This altered lysosomal function is likely caused by mitochondrial dysfunction and subsequent increase in reactive oxygen species (ROS). Interestingly, cotreatment with a mitochondria-targeted antioxidant rescued the lysosomal impairment and attenuated the 27HC-mediated increase in EV secretion. Overall, our findings establish how a cholesterol metabolite regulates EV secretion and paves the way for the development of strategies to regulate cancer progression by controlling EV secretion.

Key Words: 27-hydroxycholesterol, extracellular vesicles, myeloid immune cell, lysosome, reactive oxygen species, mitochondria

Abbreviations: 27HC, 27-hydroxycholesterol; CTSB, Cathepsin B; DMSO, dimethylsulfoxide; ECAR, extracellular acidification rate; ER, estrogen receptor; ESCRT, endosomal sorting complex required for transport; EV, extracellular vesicle; FAD, flavin adenine dinucleotide; LXR, liver X receptor; MitoQ, Mitoquinol; MV, microvesicle; MVB, multivesicular body; NAD(P)H, nicotinamide adenine dinucleotide; NDUFS1, NADH:ubiquinone oxidoreductase core subunit S1; NRF1, nuclear respiratory factor 1; NTA, nanoparticle tracking analysis; OCR, oxygen consumption rate; PER, proton efflux rate; qPCR, quantitative polymerase chain reaction; ROS, reactive oxygen species; SLAM, simultaneous label-free autofluorescence multiharmonic; TBST, Tris-buffered saline with Tween; TMRM, tetramethylrhodamine methyl ester.

Extracellular vesicles (EVs) are nano-sized membrane bound vesicles that comprise biologically active cargo including proteins, lipids, and nucleic acids (1, 2). They are signaling entities involved in mediating cross talk between cells and, in this way, they behave like multisingaling hormones (3). The International Society for Extracellular Vesicles (ISEV) now defines EVs as “particles naturally released from the cell that are delimited by a lipid bilayer and cannot replicate” (4). EVs are broadly divided into 2 subgroups: small EVs or exosomes,

which fall in the size range of 30 to 150 nm and are derived from endosomes by their maturation to form multivesicular bodies (MVBs), and large EVs or microvesicles (MVs), which are in the size range of 150 to 500 nm and are formed at the plasma membrane (5). Other subtypes of EVs include exomeres (6), oncosomes (7), and apoptotic bodies (8).

EVs, in addition to other secreted factors such as chemokines and growth factors, are critical messengers in tumor progression and metastasis (9, 10). EVs influence cancer progression

by transporting molecules that can initiate several pathophysiological processes such as vascular leakiness, angiogenesis, and formation of the premetastatic niche (11, 12). Therapeutic targeting of EVs and EV cargo could provide an approach to impair metastasis. Several factors, such as post-translational modifications (13, 14), hypoxia (15, 16), proto-oncogenes, and oncogenes (17, 18) and metabolic changes, such as alterations in rates of glycolysis and oxidative phosphorylation (19, 20), have been implicated in modulating EV secretion as well as EV cargo. Targeting of these regulatory pathways may serve as a means to impair the secretion of cancer-promoting EVs and thus act as potential therapeutic strategies for cancer. Specifically, pathways that alter EV secretion may be prime targets for such intervention. However, neither the metabolic or endocrine agents that regulate EV secretion, nor the mechanisms by which EV secretion is regulated, are fully understood.

Elevated cholesterol has been identified as a poor prognostic factor for breast cancer patients and cholesterol lowering drugs such as statins have been associated with increased recurrence-free survival (21). The cholesterol metabolite 27-hydroxycholesterol (27HC) is an endogenous oxysterol that has been shown to mediate many of the pro-tumor effects of cholesterol (22-24). Physiologically, 27HC acts as a regulator of cholesterol homeostasis, through feedback inhibition of cholesterol biosynthesis, promotion of cholesterol catabolism and through increased cellular cholesterol efflux (25). However, in the context of breast cancer, 27HC has been shown to increase the proliferation of estrogen receptor positive (ER+) cancer cells in an ER dependent manner (22). In addition, 27HC treatment of metastasis-bearing mice led to increased myeloid immune cell infiltration, and a decrease of intratumoral CD8+ cytotoxic T cells (23). Mechanistically, one way in which 27HC promotes breast cancer progression is through its action on liver X receptors (LXRs) in myeloid cells, resulting in suppression of T-cell expansion (24). Collectively, these studies strongly implicate the involvement of 27HC and myeloid immune cells in the progression of breast cancer.

Interestingly, while exploring how 27HC alters myeloid immune cell function, we found that the treatment of several cell types with 27HC resulted in an increased rate of EV secretion and altered EV cargo (26). Simultaneous label-free autofluorescence multiharmonic (SLAM) microscopy indicated that EVs from 27HC-treated cells had a decreased ratio of flavin adenine dinucleotide (FAD) to (FAD + nicotinamide adenine dinucleotide [NAD(P)H]) compared with those from dimethylsulfoxide (DMSO)-treated cells, suggesting that the cargo was altered (26). Importantly, primary tumor and metastatic burden was increased in mice treated with EVs derived from myeloid immune cells incubated with 27HC, findings that were consistent in 2 different murine mammary cancer models, 4T1 and Met1 (26). Given that EVs secreted post-27HC treatment are pro-tumorigenic, our objective was to elucidate the mechanism by which 27HC increases the biogenesis of these EVs.

Here we have established that 27HC increases EV secretion by altering lysosomal homeostasis, leading to MVBs being directed away from lysosomal degradation and toward secretion as EVs. We have also observed that the altered lysosomal function is caused in part by 27HC-mediated mitochondrial disruption and subsequent production of reactive oxygen species. Further, we have observed that cotreatment of 27HC with

Mitoquinol (MitoQ), a mitochondria-targeted antioxidant, is able to rescue the disrupted lysosomal homeostasis and therefore attenuate the 27HC-mediated increase in EV secretion. Overall, we have delineated a mechanism causing the increased secretion of EVs.

Materials and Methods

Reagents

27HC (purity 95%) was synthesized by Sai Labs (Hyderabad, India). Bafilomycin A and Mitoquinol were purchased from Cayman Chemicals (Ann Arbor, MI). All compounds were dissolved in DMSO and stored at -20°C .

Cell Culture

Murine cell lines RAW 264.7 and J774A.1 were purchased from the American Type Culture Collection (ATCC, USA) and were cultured in Dulbecco's Modified Eagle Medium (DMEM, Gibco, USA) media, supplemented with 10% fetal bovine serum (FBS, Gibco), 1% Non-essential amino acids (Corning), 1% Sodium Pyruvate (Corning) and 1% Penicillin/Streptomycin (Corning). Briefly, cells were seeded and treated with the respective compounds for 24 hours in media containing EV-depleted FBS (Gibco). All cells were maintained at 37°C with 5% CO_2 . Cell lines were cultured no longer than passage 25. Cell lines were routinely tested for mycoplasma.

EV Isolation

EVs were isolated from cell culture supernatant using one of the two independent methods. For nanoparticle tracking analysis (NTA), EVs were enriched using ExoQuick TC ULTRA EV Isolation Kit (SBI Biosciences) as previously described (26). For NTA and Western blot analyses, EVs were enriched by differential centrifugation which collected the supernatants after 800g for 10 minutes and 2000g for 30 minutes followed by ultracentrifugation (Sorvall, Thermo Scientific) at 10 000g for 1 hour (Microvesicles or large EVs) and 100 000g for 1 hour (exosomes or small EVs). Supernatant depleted of EVs was considered as vesicle free media and used for Western blot analysis.

Nanoparticle Tracking Analysis

The concentration of EVs and their size distributions were measured using NanoSight NS300 (Malvern Panalytical). For each sample, three 30-second videos were captured and analyzed using NTA3.1 software. During capture, screen gain was set at 1.0 and camera level at 13. For analysis, screen gain was set at 10.0 and detection setting at 5.

Western Blot Analysis

For Western blot analysis of cells, lysis was carried out using RIPA lysis buffer and protein was quantified using BCA Assay (Thermo Fischer Scientific, USA). An equal amount of cell protein was used, and protein was separated using SDS-PAGE. For EVs, EV protein obtained from equal number of cells was lysed directly in Laemmli buffer and loaded into the gel. Separated proteins were transferred to PVDF membrane and blocked using 5% milk in Tris-buffered saline with Tween (TBST). The blots were incubated with primary antibody overnight at 4°C (RRID: AB_2162471, RRID:AB_2754982, RRID:AB_1279332, RRID:AB_2848144), washed using TBST, incubated with

HRP-conjugated secondary antibody for 1 hour at room temperature and washed using TBST. Heat shock protein 90 (HSP90) was used as loading control (RRID:AB_2121214). Blots were incubated with either SuperSignal West Pico or Femto chemiluminescent substrates and imaged using iBrightCL1000 imaging system (Thermo Fischer Scientific, USA).

RNA Isolation and Quantitative PCR Analysis

Total RNA was extracted from cells using GeneJet RNA Purification kit (Thermo Fischer) and cDNA was synthesized using iScript Reverse Transcription Supermix (Bio-Rad), as previously described (26). Gene expression was determined by quantitative polymerase chain reaction (qPCR), using iTaq Universal SYBR Green Supermix (Bio-Rad). The primers used were designed using Primer-Blast (<https://www.ncbi.nlm.nih.gov/tools/primer-blast/>). Expression was determined using the formula, $2^{-\Delta\Delta CT}$, and normalized to housekeeping gene, TATA box binding protein (TBP).

Immunofluorescence Microscopy

Cells were cultured in glass slides (ibidi) coated with poly-L-lysine (Sigma) and treated with respective compounds prior to being fixed and permeabilized with ice cold methanol for 5 minutes, blocked with 5% bovine serum albumin for 1 hour and then incubated with indicated primary antibodies (anti-EEA1, anti-CD63, anti-LAMP1 and anti-CTSB; 1:100; Abcam; RRID:AB_10863524, RRID:AB_2754982, RRID:AB_2923327, RRID:AB_2848144) at 4 °C overnight, followed by secondary antibody (Goat polyclonal Ab to Rabbit IgG (Alexa Fluor®488); 1:1000; RRID:AB_2630356) at room temperature for 1 hour. Samples were mounted with mounting medium containing DAPI (ibidi) and imaged using Zeiss LSM700 or LSM900 Confocal Microscope. Images were analyzed using Fiji.

(Scanning) Transmission Electron Microscopy

For analysis of MVBs using electron microscopy, cells were pelleted down and fixed using 2.0% paraformaldehyde and 2.5% glutaraldehyde (both electron microscopy grade) in 0.1 M Na-Cacodylate buffer, pH 7.4, for 4 hours at 4 °C. Samples were washed in Na-Cacodylate buffer for 10 minutes and again fixed in 1.0% aqueous osmium tetroxide for 90 minutes in the dark. Samples were washed and then stained using 2% aqueous uranyl acetate, overnight, at 4 °C. Then, samples were dehydrated using a graded ethanol series (37%, 67%, 95%) for 10 minutes each and then using 100% ethanol 3 times for 10 minutes each on a shaker. They were then infiltrated using a series of ethanol:polypropylene oxide for 10 minutes each and propylene oxide:Polybed 812 mixture (without DMP-30) for 10 minutes each, prior to embedding. Samples were then embedded in 100% Polybed 812 mixture (without DMP-30), overnight at room temperature. Then they were placed in 100% Polybed 812 mixture with 1.5% DMP-30, in molds, and into oven at 60 °C for 24 hours. Thin sections were cut using an ultramicrotome (Ultracut UCT, Leica), collected on grids and examined by electron microscopy (Tecnai G2 F20 S-Twin 200 kV, Thermo FEI).

Measurement of Number of Acidic Organelles

Acidic particles in cells were measured using LysoTracker™ Deep Red dye (Invitrogen, USA). Cells were cultured in ibidi

glass slides and treated with respective compounds. After incubation, the media was replaced with media containing the respective dye, along with Hoesht 33342 dye (Invitrogen, USA) to stain the nucleus. Samples were imaged using Zeiss LSM900 Confocal Microscope. Images were analyzed using Fiji. Signal was quantified per field of view and normalized to Hoesht.

Measurement of Cellular Oxidative Stress and Mitochondrial Function

The amount of reactive oxygen species (ROS) produced within the cell was measured using CellROX™ Deep Red Reagent for oxidative stress detection (Invitrogen, USA). The cells were cultured in glass slides (ibidi) coated with poly-L-lysine (Sigma) and treated with respective compounds. CellROX reagent was added to media, along with Hoesht 33342 dye (Invitrogen, USA). Samples were imaged using Zeiss LSM900 Confocal Microscope. Images were analyzed using Fiji. Signal was quantified per field of view and normalized to Hoesht. Mitochondria, mitochondrial membrane potential, and mitochondrial ROS were measured similarly using MitoTracker Deep Red, TMRM (tetramethylrhodamine methyl ester), and MitoSOX dyes.

Label-Free Imaging Using Simultaneous Label-Free Autofluorescence Multiharmonic Microscopy

Imaging of cells using SLAM microscopy was carried out as described in (26, 27). In short, cells were cultured in glass bottom dish coated with poly-L-lysine and treated with respective compounds. Cells were imaged using multiphoton microscopy with excitation centered at 110 nm with an average power of 14 mW pulse-shaped beam to excite the sample and NAD(P)H and FAD signals were captured using 420 to 480 nm and 580 to 640 nm filter, at a spatial resolution of < 500 nm.

Seahorse Assay

Cells were seeded in XFe96 cell culture microplates (Agilent, USA) and treated with compounds for 24 hours. Cells were washed with Seahorse XF DMEM assay buffer (Agilent, USA) supplemented with 10 mM glucose, 1 mM pyruvate, and 2 mM glutamine, and incubated for 1 hour at 37 °C without CO₂. The ATP production from mitochondrial respiration and glycolytic respiration in response to Oligomycin and Rotenone/Antimycin A was measured using the ATP production assay kit (Agilent, USA). The oxygen consumption rate (OCR) and extracellular acidification rate (ECAR) from mitochondrial oxidative phosphorylation in response to Oligomycin, Carbonyl cyanide-p-trifluoromethoxyphenylhydrazone (FCCP) and Rotenone/Antimycin A was measured using the mitochondrial stress test kit (Agilent, USA). The glycolytic activity or glycoPER (glycolytic proton efflux rate) in response to Rotenone/Antimycin A and 2-deoxy-D-glucose was measured using glycolytic rate assay (Agilent, USA). All measurements were performed using Seahorse XFe96 Bioanalyzer (Agilent, USA).

Statistical Analysis

All statistical analysis was performed using GraphPad Prism software. Data are presented as mean ± SEM. Statistical measurement was carried out using the Student *t* test for 2 groups

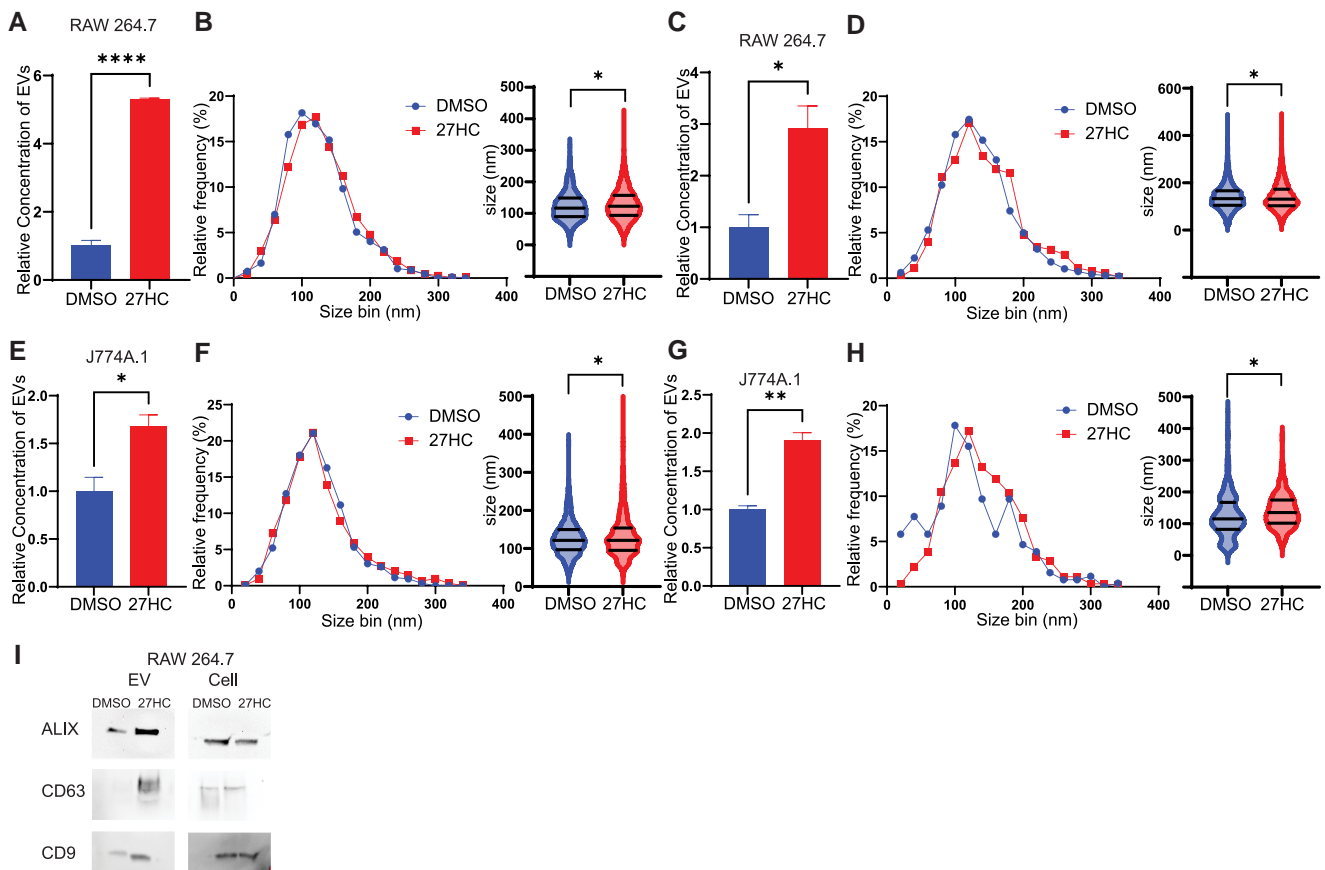


Figure 1. 27-Hydroxycholesterol (27HC) promotes EV secretion from cell line models of myeloid immune cells. EVs were collected from conditioned media of RAW 264.7 cells (A-D) and J774A.1 cells (E-H), using 2 different EV isolation techniques (ultracentrifugation and ExoQuick kit). The number of particles and size distribution were measured by nanoparticle tracking analysis (NTA) using NanoSight NS300 ($n = 3/\text{condition}$). For B, D, E, and H: the size distribution is shown as a histogram to the left, and a violin plot to the right. On the violin plots, the central black line is the median and the upper and lower black lines denote the quartiles. (I) EVs were characterized for standard EV markers using Western blot. EVs from equal number of cells were used for the blots. Statistical analyses were performed using the Student *t* test. *****P* value < .0001, ***P* value < .01, **P* value < .05. Data are presented as mean \pm SEM.

and using Ordinary one-way ANOVA with Dunnett multiple comparison test for more than 2 groups. A *P* value < .05 was considered statistically significant.

Results

27-Hydroxycholesterol Promotes EV Secretion in 2 Different Myeloid Immune Cell Lines

We have previously shown that 27HC stimulated EV secretion in myeloid immune cells and that the EVs from 27HC-treated myeloid cells had a different size profile. Here, we explored the extent of this regulation by examining its effects in 2 different cell line models of myeloid cells: RAW 264.7 and J774.A1. The RAW264.7 line is a monocyte/macrophage-like line derived from a tumor induced by the Abelson murine leukemia virus and is a very commonly used mouse “macrophage” line in medical research (28, 29). J774.A1 are derived from a female mouse with reticular cell sarcoma and have monocyte/macrophage morphology and have been used to explore various macrophage functions (30-32). Therefore, we first wanted to explore whether the regulation of EV secretion by 27HC extended to these different myeloid cell models.

Cells were treated with 27HC (10 μM) for 24 hours, the EC_{50} of 27HC for either the estrogen receptor or liver X

receptor being around 1 μM (33, 34). As expected, 27HC upregulated the expression of LXR target genes *Abca1* and *Abcg1*. Since 27HC is a selective LXR modulator, it did not upregulate *Srebf1* or *Fasn*, while a synthetic agonist (GW3965) did (35) (Supplementary Fig. S1 found at (36)). EVs were isolated from the conditioned media using ultracentrifugation, considered the gold standard of EV enrichment. Nanoparticle tracking analysis (NTA) of EV particle number and size distribution indicated that 27HC treated RAW 264.7 cells resulted in increased EV secretion (Fig. 1A). Furthermore, the particle size distribution was shifted toward a slightly larger size (Fig. 1B). These findings were also found when EVs were isolated using a commercial kit (ExoQuick, Fig. 1C and 1D). Importantly, similar findings were observed when using the J774A.1 model, indicating that 27HC-induced EV secretion is not cell line specific (Fig. 1E-1H). We characterized these EVs as expressing the classic EV tetraspanin markers CD63 and CD9, as well as ALIX (Fig. 1I). These data are consistent with our previously published findings, where EVs from RAW 264.7 cells were characterized using flow cytometry for tetraspanins and transmission electron microscopy for ultrastructure (37). Therefore, we conclude that RAW264.7 and J774A.1 cell lines are a suitable model to explore the mechanisms by which 27HC stimulates EV biogenesis.

27-Hydroxycholesterol Treatment Does Not Alter Genes Associated With Endosome Formation, but Leads to the Enlargement of Multivesicular Bodies

EVs are a heterogeneous population consisting of exosomes and microvesicles. Although still understudied, the process of EV biogenesis begins with the formation of early endosomes at the plasma membrane, which then form late endosomes. A complex machinery called the *endosomal sorting complex required for transport* (ESCRT) is recruited for the sorting of cargo. The endosome then matures to form multivesicular bodies (MVBs) containing intraluminal vesicles (38, 39). These MVBs can either be degraded in the lysosome or, with the help of Rab and SNARE transport proteins, dock at the plasma membrane and release the intraluminal vesicles as exosomes (3, 40-42). Microvesicles are formed by outward budding and fission at the plasma membrane (42-44).

To determine the mechanism by which 27HC modulates EV secretion, we first analyzed the expression of several genes associated with the biogenesis of EVs, expecting that an upregulation of these genes would be required for increased biogenesis. We found that 27HC does not significantly upregulate the expression of genes encoding ESCRT components (Fig. 2A), in either RAW264.7 or J774A.1 cells. This indicates that either the modulation of ESCRT is not at the mRNA level or does not involve ESCRT in its regulation of EV biogenesis.

Therefore, we next focused on biogenesis mechanisms downstream of the ESCRT pathway. Immunofluorescence analysis of the endosome marker EEA1 indicated that 27HC did not change the total intensity or the size of EEA1-positive early endosomes, suggesting that the regulation is not at the endosomal level (Fig. 2B). However, 27HC did increase the levels of the MVB marker CD63 and increased the size of the CD63-positive MVBs, as assessed by immunofluorescence (Fig. 2C). Transmission electron microscopy also revealed an enlargement in the size of vesicular bodies within the cells (Fig. 2D). Interestingly, when the MV fraction of ultracentrifuged conditioned media was assessed, 27HC was found to also increase the presence and size of these larger particles (Fig. 2E-2H). Collectively, these data suggest that the mechanism by which 27HC increases EV secretion is likely to (i) impact the secretion of both small and large EVs; and (ii) be downstream of the ESCRT complex.

27-Hydroxycholesterol Alters Lysosomal Function

Thus far, our data indicate that 27HC increases the secretion of both small and large EVs and that it seems to work downstream of the ESCRT complex. This points to a mechanism whereby treatment with 27HC leads to the secretion of EVs that would otherwise have been targeted toward lysosomal degradation. We have observed that 27HC increases MVB size (Fig. 2C and 2D). This indicates that there is less degradation and recycling of the MVBs within the cell and instead, the MVB cargo is being released as EVs. Interestingly, there have been several reports that an increase in MVB size can result from decreased trafficking of MVBs toward the lysosome (13, 45). Lysosomes are a crucial regulatory component of the cell and are involved in maintaining cellular homeostasis by actively degrading and recycling intracellular components and are also involved in regulating cellular signaling and metabolism (46, 47). Lysosomes act as the fate determining step for MVBs once they are formed; MVBs can either fuse with the lysosome and get degraded, where the cargo gets recycled

within the cell, or the MVBs can fuse with the plasma membrane and release their contents as EVs (48). To study the effect of 27HC on lysosomes, we stained for LAMP1, which is a lysosomal marker, and observed no significant decrease in the overall LAMP1 signal intensity in the cell (Fig. 3A). However, there was an increase in the size of those lysosomes remaining after 27HC treatment (Fig. 3A).

An increase in the size of lysosomes has been suggested to occur as a result of lysosomal membrane permeabilization, where the integrity of the lysosomal membrane is disrupted, leading to a release of lysosomal components into the cytosol as well as their secretion into the extracellular space/media (49). If lysosomal membrane integrity is impaired by 27HC or if 27HC promotes lysosome exocytosis, we would expect an increase in lysosomal proteins secreted by the cells. Thus, we measured the expression of a lysosomal protease, Cathepsin B (CTSB), expecting that if lysosome homeostasis was disrupted there would be a change in CTSB protein. Using immunofluorescence, we found that 27HC significantly increased CTSB at the cellular level (Fig. 3B). CTSB is produced as pro-CTSB (unprocessed form) and gets cleaved in the lysosome to form active CTSB (processed form). We observed an increase in the unprocessed form of the protein by Western blot analysis, suggesting that although 27HC increases CTSB, its lysosomal processing is impaired (Fig. 3C). We also observed an increase in the amount of CTSB protein in the conditioned media depleted of EVs (vesicle free media), indicating that the CTSB is either escaping the lysosome or there is increased lysosomal exocytosis, both resulting in extracellular secretion (Fig. 3D). Interestingly, the mRNA expression of CTSB was also increased by treatment of RAW cells with 27HC, suggesting that there may be feedback to replenish CTSB levels (Fig. 3E). Collectively, these data indicate that the lysosome homeostasis is altered, disrupting normal CTSB processing and secretion, and there are likely feedback mechanisms engaged to increase CTSB synthesis.

Lysosomes are also important for the process of autophagy, where autophagosomes transfer cytosolic contents to the lysosome by fusion to form autolysosome, and the contents get recycled within the cell (50). We observed that 27HC treatment leads to an increase in the amount of LC3b positive vesicles or autophagosomes within the cells (Fig. 3F), again suggesting lysosomal dysfunction is decreasing autophagosome processing. In summary, the data presented in Fig. 3 strongly support our hypothesis that lysosomal function is being impaired by 27HC.

27-Hydroxycholesterol Induces Lysosomal Dysfunction Leading to an Impaired Acidification of Lysosomes and Increased EV Secretion

To further study the effect of 27HC on lysosomes, we assessed its effect on lysosomal acidification. First, we assayed the number of acidic organelles in the cells using a LysoTracker probe, which is a cell-permeable fluorescent dye that stains acidic organelles such as the lysosome. The probe acts as a lysosomotropic; it diffuses across the plasma membrane and enters the acidic lysosomes, where it gets protonated and localized within the organelle. A decrease in LysoTracker signal was observed in cells treated with 27HC, indicating fewer acidic organelles (Fig. 4A). This finding indicates that lysosomes were failing to properly maintain their acidity, providing further support for 27HC disrupting lysosomal function.

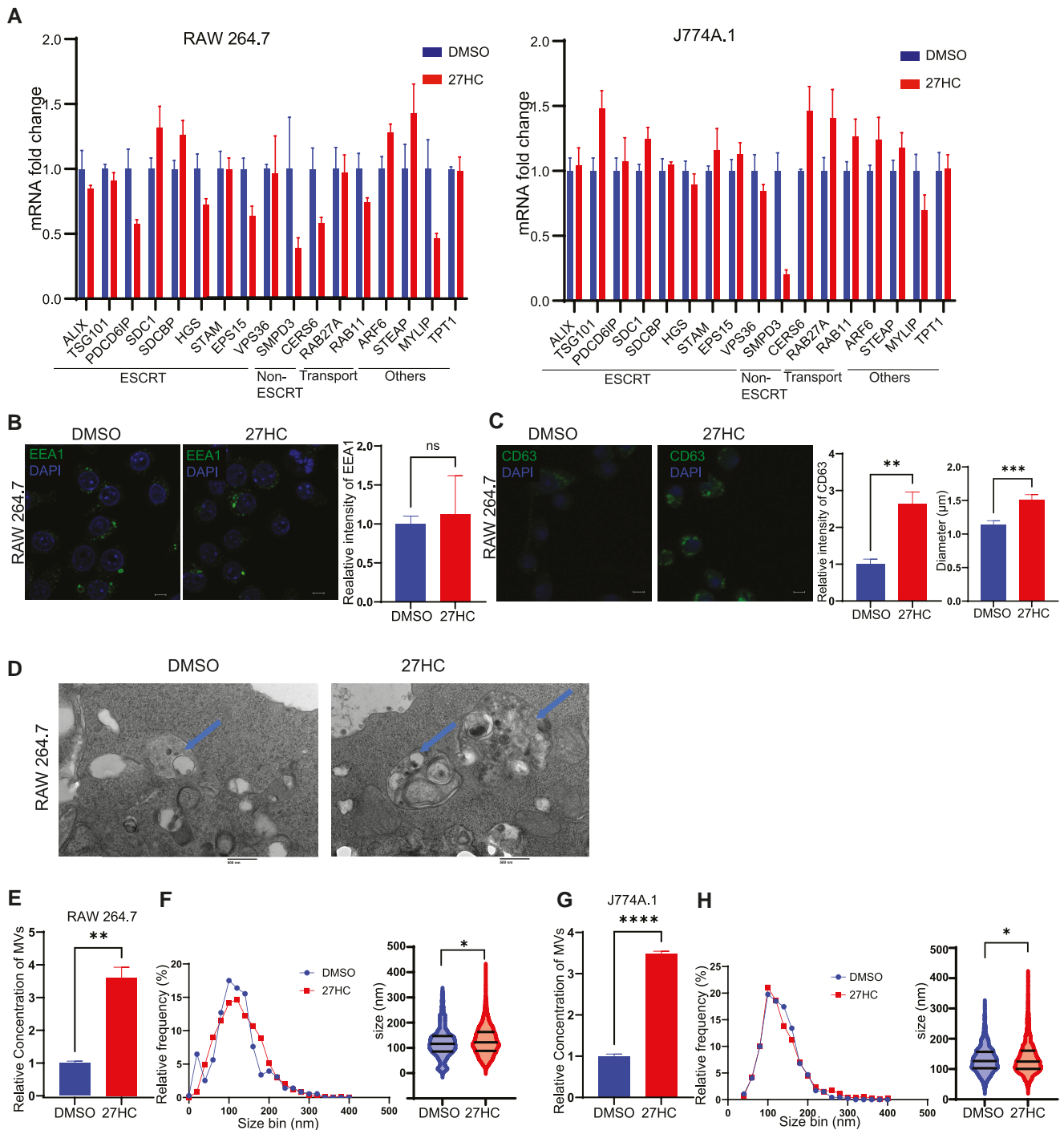


Figure 2. 27HC treatment does not alter genes associated with endosome formation, but it leads to the enlargement of multivesicular bodies (MVBs). (A) mRNA expression of several ESCRT-related, non-ESCRT-related, and other genes associated with EV biogenesis indicates that 27HC does not lead to increased expression. RAW 264.7 or J774A.1 cells were treated with DMSO (control) or 27HC for 24 hours prior to assessment of mRNA by RT-qPCR. (B) Confocal microscopy analysis of Early Endosomal marker, EEA1 indicating that 27HC does not alter the amount of early endosomes. Scale bar, 5 µm. Right graph: quantification of EEA1 signal relative to DAPI (n = 4). Each data point corresponds to the intensity of EEA1 signal per field of view. (C) Confocal microscopy analysis of MVB marker, CD63 indicating that 27HC increases the amount of CD63 intensity per cell and increases the size of CD63 positive MVBs in the cells. Scale bar, 5 µm. Right graphs: quantification of CD63 signal relative to DAPI (n = 3) and size of CD63 positive MVBs (n = 20 dots). Each data point corresponds to the intensity of CD63 per field of view and size of CD63 positive MVBs. (D) (Scanning) transmission electron microscopy of cells treated with DMSO (control) or 27HC, indicating enlarged MVBs (arrows) Scale bar, 100 nm. (E-H) EVs obtained from the 10k ultracentrifugation fraction indicating increase in number of particles and size distribution in RAW 264.7 cells and J774A.1 cells, on treatment with 27HC. For F and H: the size distribution is shown as a histogram to the left, and a violin plot to the right. On the violin plots, the central black line is the median and the upper and lower black lines denote the quartiles. Statistical analyses were performed using a Student t test. ****P value < .0001, ***P value < .001, **P value < .01, *P value < .05. Data are presented as mean ± SEM. Original confocal images were used for analysis and representative images depicted here were brightness adjusted.

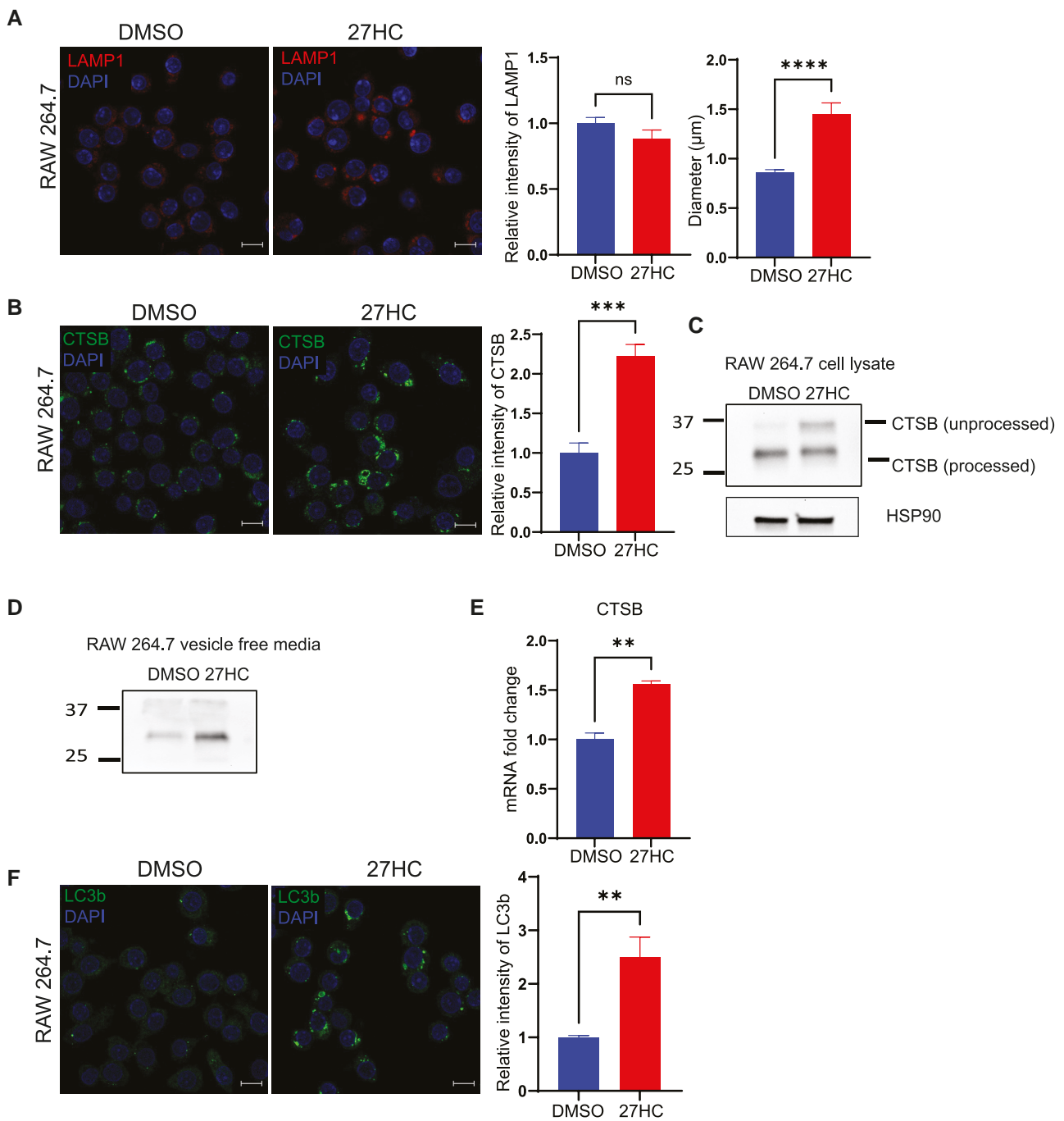


Figure 3. 27HC impairs lysosomal function. (A) Confocal microscopy analysis of lysosomal marker, LAMP1 indicating that 27HC increases the size of LAMP1 positive lysosomes in the cells. Scale bar, 5 μ m. Right graphs: quantification of LAMP1 signal relative to DAPI ($n = 5$) and size of LAMP1 positive lysosomes ($n = 20$ dots). Each data point corresponds to the intensity of LAMP1 signal per field of view and size of lysosomes. (B) Confocal microscopy analysis of Cathepsin B in cells indicating an increase in intensity of Cathepsin B protein in cells. Scale bar, 10 μ m. Right graph: quantification of Cathepsin B signal relative to DAPI ($n = 4$). Each data point corresponds to the intensity of Cathepsin B per field of view. (C) Western blot analysis of a lysosomal protease, Cathepsin B in cells indicating an increase in the unprocessed form of Cathepsin B on treatment with 27HC. (D) Western blot analysis of Cathepsin B in equal volumes of vesicle-free media indicating an increase in Cathepsin B in media. (E) Quantitative PCR of Cathepsin B (CTSB) indicating an increase in mRNA ($n = 4$). (F) Confocal microscopy analysis of autophagy marker LC3b in cells indicating an increase in intensity of LC3b positive autophagosomes in cells. Scale bar, 10 μ m. Right graph: quantification of LC3b signal relative to DAPI ($n = 6$). Each data point corresponds to the intensity of LC3b per field of view. Statistical analyses were performed using a Student *t* test. *****P* value < .0001, ****P* value < .01, **P* value < .05. Data are presented as mean \pm SEM. Original confocal images were used for analysis and representative images depicted here were brightness adjusted.

The acidic lumen of lysosomes is in part maintained by ATP6V1A. ATP6V1A is a lysosomal V-ATPase, that functions by coupling the energy obtained from ATP hydrolysis to the transport of protons into the lysosomes (51). To study

the effect of impaired lysosomal acidification on the rate of EV secretion, we treated cells with Bafilomycin A, a known inhibitor of ATP6V1A (52). As expected, treatment with Bafilomycin A led to a decreased number of acidic organelles

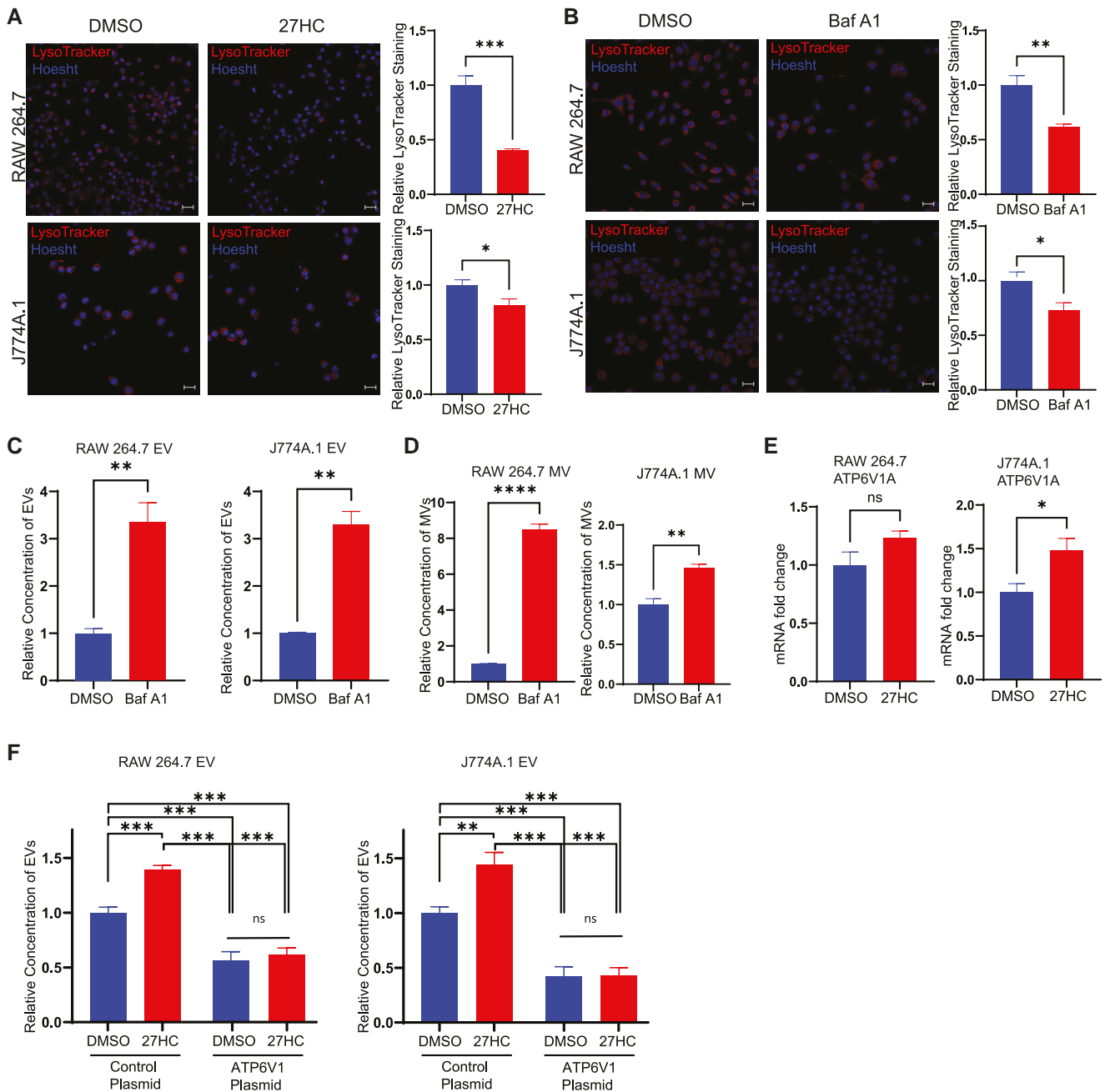


Figure 4. 27HC impairs acidification of lysosomes which leads to increased EV secretion. (A) Confocal microscopy analysis of number of acidic organelles (lysosomes) using LysoTracker Deep Red showing a decrease in signal on treatment with 27HC, indicating decreased acidic organelles. Scale bar, 20 μ m. Right graph: quantification of LysoTracker signal relative to Hoesht, per field of view (n = 4). (B) Treatment of cells with Bafilomycin A1, an inhibitor of the lysosomal V-ATPase pump ATP6V1A, lead to a decrease in number of acidic organelles (n = 4), and (C-D) an increase in secretion of EVs and MVs (n = 3). (E) Quantitative PCR of ATP6V1A indicating that 27HC does not significantly change the mRNA expression of ATP6V1A in RAW264.7 cells, but it does increase it in J774.1 cells (n = 4). (F) Overexpression of murine ATP6V1A in RAW264.7 or J774A.1 cells decreases EV secretion. While 27HC increases EV secretion in cells transfected with a control plasmid, it fails to do so in cells overexpressing ATP6V1A. Statistical analyses were performed using a Student *t* test except in (F) where 1-way ANOVA followed by a Šidák post hoc analysis was performed. *****P* value < .0001, ***P* value < .01, **P* value < .05. Data are presented as mean \pm SEM. Original confocal images were used for analysis and representative images depicted here were brightness adjusted.

(Fig. 4B). Importantly Bafilomycin A treatment increased the secretion of both small and large EVs (Fig. 4C and 4D), mirroring what we observed with 27HC treatment (Fig. 1). Our findings that Bafilomycin A treatment recapitulated the effects of 27HC lends strong support to our hypothesis that 27HC increases EV secretion by altering lysosomal function, decreasing MVB degradation by lysosomes, and ultimately shifting them toward secretion as EVs.

Recent studies have shown that a decrease in ATP6V1A mRNA levels leads to an impairment of lysosomal acidification and an increase in EV secretion (15, 45). If the pro-EV-secretory effects of 27HC were via ATP6V1A, we would expect 27HC to decrease its mRNA levels. However, when we examined the effect of 27HC on ATP6V1A mRNA levels, we observed no change in its expression in RAW 264.7 cells and an increase in expression in J774A.1 cells

(Fig. 4E). ATP6V1A upregulation appears to be a response to compensate for disrupted lysosomal homeostasis. Thus, 27HC likely acts upstream of, and not directly on the lysosome, to impair lysosomes.

To more directly evaluate whether disruption of lysosomal acidification was responsible for the 27HC-mediated increase in EV secretion, we overexpressed murine ATP6V1A in RAW264.7 or J774A.1 cells. As expected based on previous reports (15, 45), overexpression alone led to a decrease in secreted EVs (Fig. 4F). Importantly, 27HC failed to increase EV secretion in cells overexpressing ATP6V1A and presumably maintaining their ability to acidify lysosomes (Fig. 4F). Thus, these data support the hypothesis that 27HC increases EV secretion by interfering with lysosomal acidification.

27-Hydroxycholesterol Increases Intracellular Oxidative Stress and Causes Mitochondrial Dysfunction

Our data thus far support a mechanism whereby 27HC disrupts normal lysosomal homeostasis, which leads to a decreased degradation of MVBs and an increase in the secretion of EVs. Our next step was to determine what contributes to this impairment of lysosomal function. Several studies have shown that elevated levels of reactive oxygen species (ROS) result in impaired lysosomal function (53, 54). Interestingly, elevated ROS has also been found to increase EV secretion (55, 56).

27HC treatment of cells increased levels of total cellular ROS (Fig 5A). This suggests that the mechanism by which 27HC disrupts lysosomes and subsequently increases EV secretion is via the initial production of ROS. Elevated levels of ROS can be a result of several factors including mitochondrial dysfunction (57-59). Further, altered mitochondrial function has been demonstrated to disrupt the structure and function of lysosomes in a ROS dependent manner (60-62). Therefore, we studied the effect of 27HC on mitochondrial function. 27HC-treated cells had decreased total mitochondria or decreased MitoTracker signal as measured using MitoTracker dye (Fig. 5B), although altered redox or mitochondrial fusion may confound this interpretation (63). Performing GO analysis on differentially expressed genes between vehicle- and 27HC-treated bone marrow-derived macrophages revealed enrichment of 2 gene sets in the Cellular Components database that were highly related to mitochondrial function: mitochondrial matrix, and mitochondrial protein-containing complex (RNA-seq dataset described in (35), Supplementary Fig. S2A (36)). Therefore, we more closely probed the expression of select genes related to mitochondrial function and oxidative phosphorylation were surveyed. The majority of genes assessed did not change upon treatment with 27HC, or changes were inconsistent between cell types (RAW264.7 vs J774A.1 cells) (Supplementary Fig. S2B (36)). However, expression of 3 genes were changed: PGC1 α , NRF1, and NDUFS1. PGC1 α is a master regulator of oxidative phosphorylation and, as such, coordinates ROS scavenging (64, 65). PGC1 α was upregulated by 27HC, which is likely a compensatory response to the increased ROS observed after 27HC treatment (as in, PGC1 α was upregulated in response to ROS, not causative of it). Both NRF1 (Nuclear respiratory factor 1) and NDUFS1 (NADH:ubiquinone oxidoreductase core subunit S1) were downregulated by 27HC. NRF1 is a central node regulating response to redox

balance and loss of NRF1 is known to increase in ROS (66). NDUFS1 catalyzes the first step of NADH oxidation and is critical for maintaining mitochondrial stability. Loss of NDUFS1 is also associated with increased mitochondrial ROS (67). Thus, 27HC downregulation of NRF1 and/or NDUFS1 may be upstream mediators of the observed increases in ROS. Further studies are required to probe these mechanisms. TMRM staining indicated that there was also a decrease in mitochondrial membrane potential (Fig. 5C). Finally, we observed an increase specifically in mitochondrial ROS using the MitoSOX stain (Fig. 5D). ROS has been demonstrated to increase lysosome exocytosis and loss of mitochondrial function impairs lysosomes (60, 68). Therefore, cellular exposure to 27HC leads to mitochondrial dysfunction and increased ROS; the ROS potentially disrupting lysosome homeostasis and thus increasing EV secretion.

27-Hydroxycholesterol Alters Mitochondrial Metabolism

Elevated mitochondrial ROS correlates with alterations in mitochondrial bioenergetics and overall cellular metabolic output (69). To study the simultaneous effects of 27HC on oxidative phosphorylation, TCA cycle, and glycolysis within the cell, we used 2 techniques: simultaneous label-free autofluorescence multiharmonic (SLAM) microscopy, and real-time cell metabolic analysis (Seahorse Assays).

In a label-free manner, SLAM microscopy measures autofluorescence emitted by FAD and NAD(P)H in live cells. A decrease in the FAD:(FAD + NAD(P)H) ratio corresponds to an increase metabolic activity in the cells (27, 70). We observed that 27HC treatment leads to an increase in the FAD:(FAD + NAD(P)H) ratio in RAW 264.7 cells (Fig. 6A). This would be reflective of a decrease in metabolic activity in the cells.

To more specifically assess metabolic flux, we measured oxygen consumption rate (OCR; an estimate of oxidative phosphorylation) and extracellular acidification rate (ECAR; an estimate of glycolytic activity), using these to calculate the proton efflux rate (PER). For both RAW 264.7 and J774A.1 cells, 27HC decreased OCR, with smaller changes observed in ECAR and PER (Seahorse ATP Rate Assay kit; Supplementary Fig. S3A-C (36)). Using these values, mitochondrial vs glycolytic ATP production can be estimated. Notably, 27HC robustly decreased mitochondrial ATP production in both cell models, while increasing glycolytic ATP production in RAW 264.7 cells but not significantly changing glycolytic ATP production in J774A.1 (Figure 6B). This was also reflected in the total ATP production rate in an independent experiment using the Seahorse Mito Stress kit (Supplementary Fig. S3D and S3E (36)). Likewise, in an independent experiment using the Glycolytic Rate Seahorse Assay, a potential compensatory increase in estimated glycolysis was observed in RAW 264.7 cells, treated with 27HC, while no significant differences were found in J774A.1 cells (Supplementary Fig. S3F and S3G (36)). 27HC led to decreased maximum respiration rate and a reduced coupling efficiency, indicated by the Seahorse Mito stress test (Fig. 6C and 6D). Collectively, these data demonstrate that mitochondrial oxidative phosphorylation is robustly disrupted, suggesting that impaired mitochondria are responsible for the observed increases in ROS. Therefore, our data demonstrate a connection between mitochondrial function, lysosomal function, and EV secretion; 27HC resulted in impaired

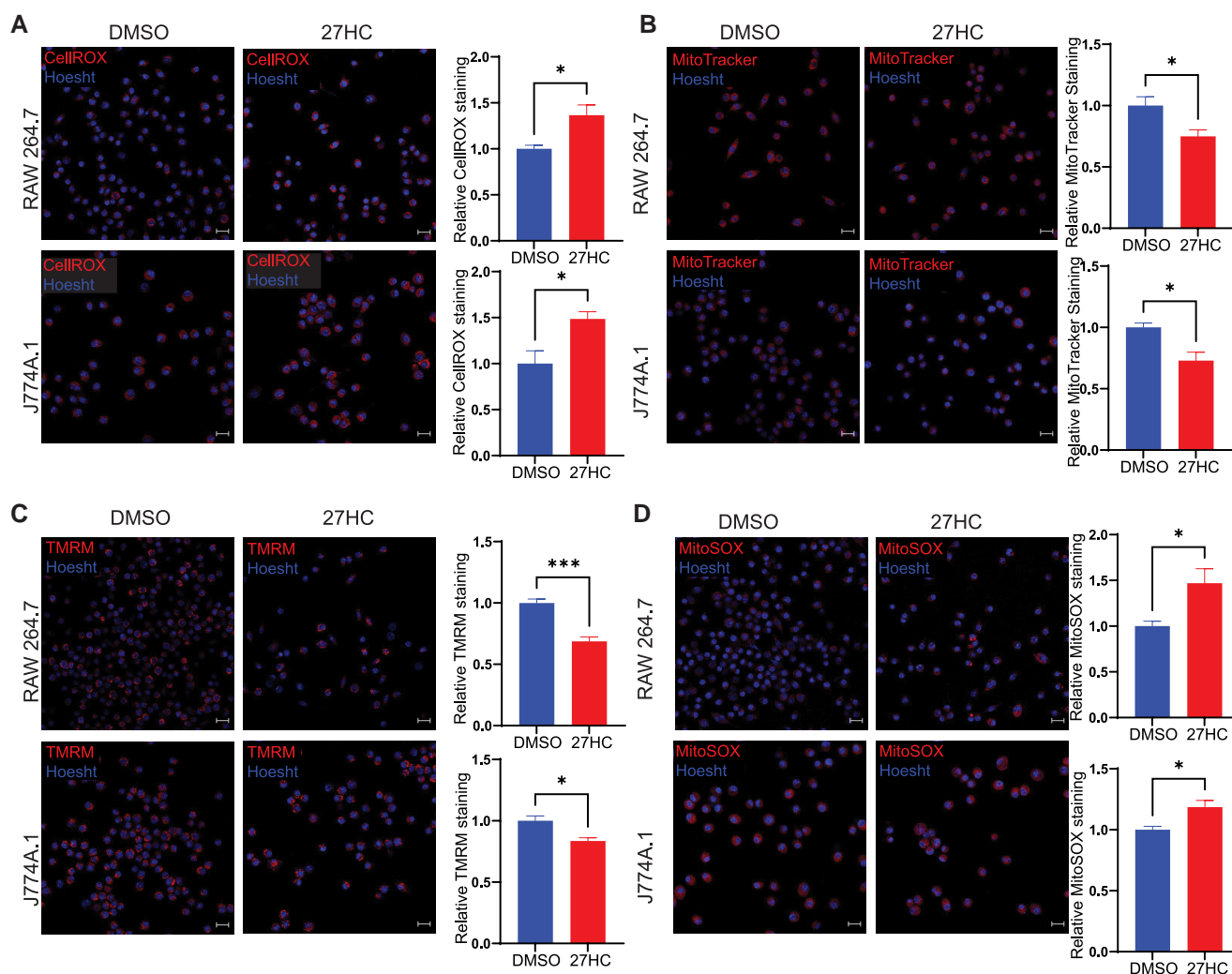


Figure 5. 27HC increases intracellular oxidative stress and causes mitochondrial dysfunction. (A) Confocal microscopy analysis of intracellular reactive oxygen species (ROS) using CellROX Deep Red indicating an increase in signal on treatment with 27HC, indicating increased levels of intracellular ROS. Scale bar, 20 μ m. Right graph: quantification of CellROX signal relative to Hoesht, per field of view (n = 4). (B) Confocal microscopy analysis of mitochondria using MitoTracker Deep Red indicating a decrease in signal on treatment with 27HC, indicating decreased mitochondrial mass. Scale bar, 20 μ m. Right graph: quantification of MitoTracker signal relative to Hoesht, per field of view (n = 4). (C) Confocal microscopy analysis of mitochondrial membrane potential using TMRM Deep Red indicating a decrease in signal on treatment with 27HC, indicating decreased mitochondrial membrane potential. Scale bar, 20 μ m. Right graph: quantification of TMRM signal relative to Hoesht, per field of view (n = 4). (D) Confocal microscopy analysis of mitochondrial ROS using MitoSOX Deep Red indicating an increase in signal on treatment with 27HC, indicating increase mitochondrial ROS production. Scale bar, 20 μ m. Right graph: quantification of MitoSOX signal per relative to Hoesht, per field of view (n = 4). Statistical analyses were performed using a Student *t* test. *****P*value < .0001, ****P*value < .001, ***P*value < .01, **P*value < .05. Data are presented as mean \pm SEM. Original confocal images were used for analysis and representative images depicted here were brightness adjusted.

mitochondrial function, increased ROS, disrupted lysosome homeostasis and thus a buildup of MVBs that are shunted toward secretion as EVs.

A Mitochondria-Targeted Antioxidant Attenuates the 27HC-Mediated Increase in EV Secretion

Our evidence thus far implicates mitochondrial ROS as the upstream initiator of the effects of 27HC on EV biogenesis. Therefore, we co-treated cells with 27HC and a mitochondria-targeted antioxidant Mitoquinol (MitoQ). MitoQ is a potent antioxidant consisting of coenzyme Q10 linked to a lipophilic triphenylphosphonium cation to enable its accumulation in the mitochondria, which blocks the generation of ROS and prevents mitochondrial oxidative damage (71, 72). We would thus expect MitoQ cotreatment to rescue the lysosomal damage.

In support of our model, MitoQ was able to normalize LysoTracker signal after a 24-hour treatment with 27HC (Fig. 7A). Importantly, MitoQ was also able to attenuate the 27HC-mediated increase in EV secretion over a 48-hour culture period (Fig. 7B). Therefore, we conclude that ROS is the upstream mediator of 27HC-stimulated EV secretion and use of an antioxidant can attenuate the increased EV secretion.

Discussion

EVs play an important role in maintaining regular cell-to-cell communication. EVs have also been strongly implicated as critical messengers in tumor progression and metastasis, in addition to other factors such as chemokines and growth factors (10, 73). These EVs influence cancer progression by transporting molecules that can initiate several pathophysiological

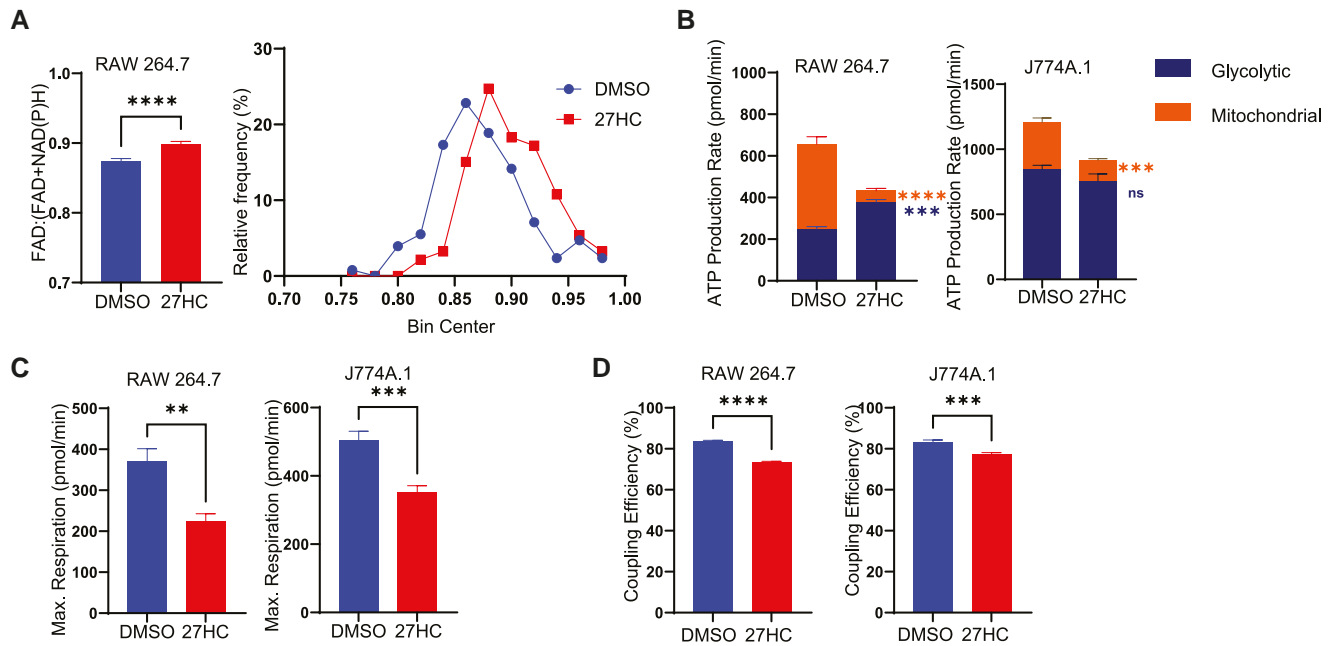


Figure 6. 27HC alters mitochondrial metabolism in myeloid cells. (A) SLAM microscopy in cells indicating an increase in FAD:(FAD + NAD(P)H) ratio in cells. (B) Seahorse ATP production assay indicating a decrease in mitochondrial ATP production ($n = 6$). (C) Seahorse Mito stress test indicating a decrease in levels of maximal respiration ($n = 6$). (D) Seahorse Mito stress test showing decreased coupling efficiency in 27HC-treated cells ($n = 6$). Statistical analyses were performed using a Student *t* test *****P* value < .0001, ****P* value < .001, ***P* value < .01. Data are presented as mean \pm SEM.

processes, such as vascular leakiness, angiogenesis, and formation of the premetastatic niche (11, 12). They also play a role in drug resistance, where the cells can directly efflux drugs via EVs (74). How or what factors regulate EV biogenesis and secretion is still poorly understood, although certain physiological stressors (eg, hypoxia) and various metabolic factors have now been found to regulate EV secretion and/or cargo (3). The regulation of EV secretion is important to understand since it represents a promising strategy for the treatment of various diseases, including cancer.

Previous work has shown that treatment of myeloid immune cells with the cholesterol metabolite 27HC leads to an increase in the secretion of EVs, and these EVs promote tumor growth and metastasis (26). Given that there is an increase in the number of EVs and these EVs have pro-tumorigenic effects, understanding the mechanisms by which their secretion is increased would provide a unique opportunity to develop intervention strategies to prevent metastatic progression. We have demonstrated here that 27HC increases EV secretion by a cascade of alterations in cellular metabolism, characterized by impaired mitochondrial function, increased cellular oxidative stress, and altered lysosomal function.

The biogenesis of EVs of endosomal origin involves the maturation of endosomes to form multivesicular bodies (MVBs) containing intraluminal vesicles which either fuse with the lysosome and get degraded or fuse with the plasma membrane and get secreted as EVs (3). Therefore, the lysosomes determine the fate of MVBs—toward degradation and recycling, or toward secretion as EVs. Lysosomes help maintain cellular homeostasis by degrading and recycling cellular components. The impairment of lysosomes leads to the inability of the cell to recycle cellular components which are generated via the endosomal-multivesicular body pathway, leading to the secretion of these contents as EVs. We have

observed here that 27HC shifts lysosomal homeostasis as measured through increased lysosomal size, decreased number of lysosomes/acidic organelles and increased secretion of cargo such as EVs. This disrupts their inability to degrade multivesicular bodies and instead leads to the secretion of their contents as EVs. Several other groups have also demonstrated that lysosomes determine the fate of MVBs. One report has shown that hypoxia promotes EV secretion by impairing lysosomal acidification (15). Another study found that a decrease in SIRT1 levels impairs lysosomal acidification and leads to secretion of EVs (45).

To further study what causes the observed change in lysosomal homeostasis, we studied the effect of 27HC on cellular ROS, since elevated levels of ROS results in impaired lysosomal function (53, 54). We observed that 27HC increases levels of cellular ROS. A majority of the ROS produced in the cell is produced by mitochondria and dysfunctional mitochondria produce elevated levels of ROS (61, 71). We have observed that 27HC impairs mitochondria and increases levels of mitochondrial ROS. Finally, since the upstream mediator for the increased EV secretion is the production of mitochondrial ROS, we co-treated the cells with a mitochondria-targeted antioxidant, Mitoquinol (MitoQ), and observed that MitoQ was able to rescue the lysosomes and attenuate the effects of 27HC on increased EV secretion.

Therefore, we have demonstrated that 27HC impairs mitochondrial function, which leads to elevated production of ROS. This elevated ROS in the cell disrupts the ability of lysosomes to degrade MVB cargo and leads to an increase in EV secretion. The use of antioxidants such as MitoQ can rescue these effects, by restoring lysosomal function and MVB degradation. Several *in vitro* and *in vivo* studies have demonstrated that MitoQ is protective against multiple diseases, including cancers (71, 75-78). Therefore, potential intervention strategies to

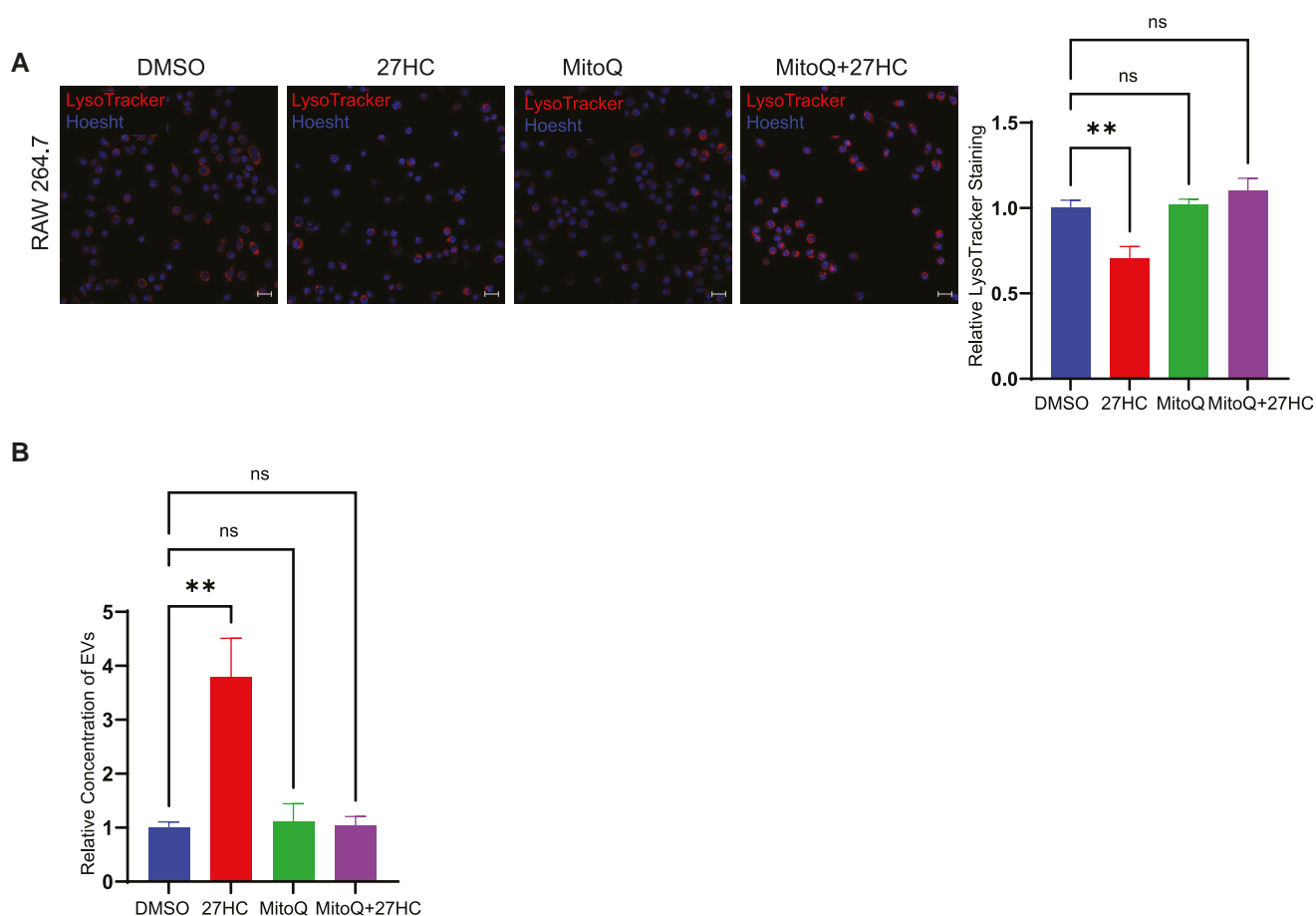


Figure 7. A mitochondria-targeted antioxidant attenuates the 27HC-mediated increase in EV secretion. (A) Confocal microscopy analysis of number of acidic organelles (lysosomes) using LysoTracker Deep Red indicating that cotreatment with MitoQ normalizes the number of acidic organelles. Scale bar, 20 μ m. Right graph: quantification of LysoTracker signal relative to Hoesht, per field of view ($n = 4$). (B) Nanoparticle tracking analysis of EVs obtained after 48 hours of treatment indicating that cotreatment with MitoQ attenuates the 27HC mediated increase in EV secretion ($n = 3$). Statistical analyses were performed using one-way ANOVA with Dunnett's multiple comparisons test. ** P value $< .01$. Data are presented as mean \pm SEM. Original confocal images were used for analysis and representative images depicted here were brightness adjusted.

attenuate the 27HC induced increase in EVs could include the use of MitoQ or other antioxidants that can prevent oxidative damage.

Cancer progression involves crosstalk between various cells in the tumor microenvironment, including immune cells, stromal cells, and fibroblasts. A vast majority of studies relating EVs and cancer progression involve the study of EVs derived from cancer cells and their influence on the functions of other cells in the tumor microenvironment (79-81). The role of immune cells in tumorigenesis is a double-edged sword. On one hand, immune cells help to enhance the antitumor immune response and act to eliminate cancer cells; while on the other, immune cells can be corrupted by cancer cells and become pro-tumorigenic. As a result, EVs from these cell types also play an important role in cancer progression. EVs from myeloid cells have been implicated in stimulating pro-metastatic properties, mediated by their interaction with other immune cells to form a suppressive tumor microenvironment (11, 82, 83). In the context of elevated cholesterol and breast cancer, we have seen that EVs derived from 27HC treated neutrophils promote breast cancer progression (26). Other studies involving immune cell-derived EVs have revealed that EVs containing miR-501-3p derived from tumor associated macrophages (TAMs) are involved in cell migration and invasion leading to

the progression of pancreatic cancer and the suppression of this miRNA in cells can inhibit this progression (84). TAMs can also promote invasion of breast cancer cells by transfer of miR-223 via the Mef2c- β -catenin pathway (85). Macrophage-derived EVs can reverse breast cancer cell quiescence and induce proliferation, leading to re-emergence from dormancy (86).

Altered cholesterol metabolism has been strongly associated with the progression of various diseases. Interestingly, several miRNAs have been implicated in the regulation of cholesterol homeostasis (87). Furthermore, cholesterol derivatives other than 27HC have also been found to alter EV secretion with altered cargo. For example, dendrogenin A was found to stimulate cancer cells to secrete EVs carrying altered cargo that increased dendritic cell maturation and Th1 T lymphocyte polarization (88). When considering our work along with other published studies, it becomes clear that EVs play an important role in the progression of cancer, but that more insights into their regulation are required for clinical translation of this knowledge.

Understanding the mechanisms that cells use to modulate EV secretion has been a long-standing goal in understanding normal cellular physiology, as well as changes in diseases such as cancer. Overall, a more comprehensive understanding

of the regulation of EV secretion will help open avenues in identifying targets that can be modulated to rescue the increase in EV secretion. Our work has demonstrated the effect of elevated levels of a cholesterol metabolite, 27HC, in increasing EV secretion. This knowledge will help identify targets or metabolites in patients as prognostic markers for diseases such as cancer and other metabolic diseases and act as druggable targets as a therapeutic strategy.

Acknowledgments

The Cancer Center at Illinois Tumor Engineering and Phenotyping Shared Resource (TEP) provided certain cell lines, routine mycoplasma testing and Seahorse XF assays (directed and assisted by Hui Xu and Huimin Zhang). Transmission electron microscopy was performed by Catherine L. Wallace at the Beckman Institute Imaging Technology Group Microscopy Suite.

Funding

U.S. Department of Defense Era of Hope Scholar Award BC200206/W81XWH-20-BCRP-EOHS (E.R.N.). National Institutes of Health grant R01 CA234025 (E.R.N.). National Institutes of Health grant T32 GM136629 (H.E.V.G.). National Institutes of Health grant T32 ES007326 (A.T.N.). National Institutes of Health grant P41 EB031772 (S.A.B.). Cancer Scholars for Translational and Applied Research (C*STAR) Program sponsored by the Cancer Center at Illinois and the Carle Cancer Center CST EP012023 (H.E.V.G.). Postdoctoral Fellows Program at the Beckman Institute for Advanced Science and Technology (N.K.). School of Molecular and Cellular Biology Summer Undergraduate Research Fellowship (H.K.).

Author Information

Erik R. Nelson is an Editorial Board Member for *Endocrinology* and played no role in the Journal's evaluation of the manuscript.

Disclosures

The authors have nothing to disclose.

Data Availability

Some or all datasets generated during and/or analyzed during the current study are not publicly available but are available from the corresponding author on reasonable request.

References

- Kalluri R, LeBleu VS. The biology, function, and biomedical applications of exosomes. *Science* (1979). 2020;367(6478):eaau6977.
- Thery C, Zitvogel L, Amigorena S. Exosomes: composition, biogenesis and function. *Nat Rev Immunol*. 2002;2(8):569-579.
- Gupta D, Krawczynska A, Nelson N. Extracellular vesicles—the next frontier in endocrinology. *Endocrinology*. 2021;162(10):bqab133.
- Welsh JA, Goberdhan DCI, O'Driscoll L, et al. Minimal information for studies of extracellular vesicles (MISEV2023): from basic to advanced approaches. *J Extracell Vesicles*. 2024;13(2):e12404.
- Raposo G, Stoorvogel W. Extracellular vesicles: exosomes, microvesicles, and friends. *J Cell Biol*. 2013;200(4):373-383.
- Zhang H, Freitas D, Kim HS, et al. Identification of distinct nanoparticles and subsets of extracellular vesicles by asymmetric flow field-flow fractionation. *Nat Cell Biol*. 2018;20(3):332-343.
- Meehan B, Rak J, Di Vizio D. Oncosomes—large and small: what are they, where they came from? *J Extracell Vesicles*. 2016;5(1):33109.
- Battistelli M, Falcieri E. Apoptotic bodies: particular extracellular vesicles involved in intercellular communication. *Biology (Basel)*. 2020;9(1):21.
- Kalluri R. The biology and function of exosomes in cancer. *J Clin Invest*. 2016;126(4):1208-1215.
- Costa-Silva B, Aiello NM, Ocean AJ, et al. Pancreatic cancer exosomes initiate pre-metastatic niche formation in the liver. *Nat Cell Biol*. 2015;17(6):816-826.
- Becker A, Thakur BK, Weiss JM, Kim HS, Peinado H, Lyden D. Extracellular vesicles in cancer: cell-to-cell mediators of metastasis. *Cancer Cell*. 2016;30(6):836-848.
- Hu M, Kenific CM, Boudreau N, Lyden D. Tumor-derived nanoseeds condition the soil for metastatic organotropism. *Semin Cancer Biol*. 2023;93:70-82.
- Villarroya-Beltri C, Baixauli F, Mittelbrunn M, et al. ISGylation controls exosome secretion by promoting lysosomal degradation of MVB proteins. *Nat Commun*. 2016;7(1):13588.
- Fei X, Li Z, Yang D, et al. Neddylation of Coro1a determines the fate of multivesicular bodies and biogenesis of extracellular vesicles. *J Extracell Vesicles*. 2021;10(12):e12153.
- Wang X, Wu R, Zhai P, et al. Hypoxia promotes EV secretion by impairing lysosomal homeostasis in HNSCC through negative regulation of ATP6V1A by HIF-1alpha. *J Extracell Vesicles*. 2023;12(2):e12310.
- Wang T, Gilkes DM, Takano N, et al. Hypoxia-inducible factors and RAB22A mediate formation of microvesicles that stimulate breast cancer invasion and metastasis. *Proc Natl Acad Sci U S A*. 2014;111(31):E3234-E3242.
- Hikita T, Kuwahara A, Watanabe R, Miyata M, Oneyama C. Src in endosomal membranes promotes exosome secretion and tumor progression. *Sci Rep*. 2019;9(1):3265.
- Imjeti NS, Menck K, Egea-Jimenez AL, et al. Syntenin mediates SRC function in exosomal cell-to-cell communication. *Proc Natl Acad Sci U S A*. 2017;114(47):12495-12500.
- Ludwig N, Yerneni SS, Menshikova EV, Gillespie DG, Jackson EK, Whiteside TL. Simultaneous inhibition of glycolysis and oxidative phosphorylation triggers a multi-fold increase in secretion of exosomes: possible role of 2'3'-cAMP. *Sci Rep*. 2020;10(1):6948.
- Wei Y, Wang D, Jin F, et al. Pyruvate kinase type M2 promotes tumour cell exosome release via phosphorylating synaptosome-associated protein 23. *Nat Commun*. 2017;8(1):14041.
- Baek AE, Nelson ER. The contribution of cholesterol and its metabolites to the pathophysiology of breast cancer. *Horm Cancer*. 2016;7(4):219-228.
- Nelson ER, Wardell SE, Jasper JS, et al. 27-Hydroxycholesterol links hypercholesterolemia and breast cancer pathophysiology. *Science* (1979). 2013;342(6162):1094-1098.
- Baek AE, Yu Y-RA, He S, et al. The cholesterol metabolite 27-hydroxycholesterol facilitates breast cancer metastasis through its actions on immune cells. *Nat Commun*. 2017;8(1):864.
- Ma L, Wang L, Nelson AT, et al. 27-Hydroxycholesterol acts on myeloid immune cells to induce T cell dysfunction, promoting breast cancer progression. *Cancer Lett*. 2020;493:266-283.
- Ma L, Nelson ER. Oxysterols and nuclear receptors. *Mol Cell Endocrinol*. 2019;484:42-51.
- Baek AE, Krawczynska N, Gupta D, et al. The cholesterol metabolite 27-hydroxycholesterol increases the secretion of extracellular vesicles which promote breast cancer progression. *Endocrinology*. 2021;162(7):bqab095.
- You S, Tu H, Chaney EJ, et al. Intravital imaging by simultaneous label-free autofluorescence-multiharmonic microscopy. *Nat Commun*. 2018;9(1):2125.

28. Raschke WC, Baird S, Ralph P, Nakoinz I. Functional macrophage cell lines transformed by Abelson leukemia virus. *Cell*. 1978;15(1):261-267.
29. Hartley JW, Evans LH, Green KY, *et al.* Expression of infectious murine leukemia viruses by RAW264.7 cells, a potential complication for studies with a widely used mouse macrophage cell line. *Retrovirology*. 2008;5(1):1.
30. Johnson BK, Abramovitch RB. Macrophage infection models for *Mycobacterium tuberculosis*. *Methods Mol Biol*. 2015;1285:329-341.
31. Ralph P, Nakoinz I. Phagocytosis and cytolysis by a macrophage tumour and its cloned cell line. *Nature*. 1975;257(5525):393-394.
32. Lam J, Herant M, Dembo M, Heinrich V. Baseline mechanical characterization of J774 macrophages. *Biophys J*. 2009;96(1):248-254.
33. Nelson ER, DuSell CD, Wang X, *et al.* The oxysterol, 27-hydroxycholesterol, links cholesterol metabolism to bone homeostasis through its actions on the estrogen and liver X receptors. *Endocrinology*. 2011;152(12):4691-4705.
34. DuSell CD, Umetani M, Shaul PW, Mangelsdorf DJ, McDonnell DP. 27-hydroxycholesterol is an endogenous selective estrogen receptor modulator. *Molecular endocrinology*. 2008;22(1):65-77.
35. Ma L, Vidana Gamage HE, Tiwari S, *et al.* The liver X receptor is selectively modulated to differentially alter female mammary metastasis-associated myeloid cells. *Endocrinology*. 2022;163(7):bqac72.
36. Nelson ER. Supplementary Data for the manuscript "Cholesterol Metabolite 27-Hydroxycholesterol Enhances the Secretion of Extracellular Vesicles by a Mitochondrial ROS-Induced dysregulation of Lysosomes". Mendeley Data, V1. doi:10.17632/9n4s2mng7x.1. 2025.
37. Baek AE, Krawczynska N, Gupta D, *et al.* The cholesterol metabolite 27HC increases secretion of extracellular vesicles which promote breast cancer progression. *Endocrinology*. 2021;162(7):bqab095.
38. Babst M, Katzmann DJ, Snyder WB, Wendland B, Emr SD. Endosome-associated complex, ESCRT-II, recruits transport machinery for protein sorting at the multivesicular body. *Dev Cell*. 2002;3(2):283-289.
39. Bache KG, Brech A, Mehlum A, Stenmark H. Hrs regulates multivesicular body formation via ESCRT recruitment to endosomes. *J Cell Biol*. 2003;162(3):435-442.
40. Colombo M, Moita C, van Niel G, *et al.* Analysis of ESCRT functions in exosome biogenesis, composition and secretion highlights the heterogeneity of extracellular vesicles. *J Cell Sci*. 2013;126(Pt 24):5553-5565.
41. Clancy JW, Sedgwick A, Rosse C, *et al.* Regulated delivery of molecular cargo to invasive tumour-derived microvesicles. *Nat Commun*. 2015;6(1):6919.
42. Clancy JW, Zhang Y, Sheehan C, D'Souza-Schorey C. An ARF6-Exportin-5 axis delivers pre-miRNA cargo to tumour microvesicles. *Nat Cell Biol*. 2019;21(7):856-866.
43. Muralidharan-Chari V, Clancy J, Plou C, *et al.* ARF6-regulated shedding of tumor cell-derived plasma membrane microvesicles. *Curr Biol*. 2009;19(22):1875-1885.
44. Bianco F, Perrotta C, Novellino L, *et al.* Acid sphingomyelinase activity triggers microparticle release from glial cells. *EMBO J*. 2009;28(8):1043-1054.
45. Latifkar A, Ling L, Hingorani A, *et al.* Loss of sirtuin 1 alters the secretome of breast cancer cells by impairing lysosomal integrity. *Dev Cell*. 2019;49(3):393-408.e7.
46. Amaral O, Martins M, Oliveira AR, Duarte AJ, Mondrago-Rodrigues I, Macedo MF. The biology of lysosomes: from order to disorder. *Biomedicine*. 2023;11(1):213.
47. Settembre C, Perera RM. Lysosomes as coordinators of cellular catabolism, metabolic signalling and organ physiology. *Nat Rev Mol Cell Biol*. 2024;25(3):223-245.
48. McAndrews KM, Kalluri R. Mechanisms associated with biogenesis of exosomes in cancer. *Mol Cancer*. 2019;18(1):52.
49. Wang F, Gomez-Sintes R, Boya P. Lysosomal membrane permeabilization and cell death. *Traffic*. 2018;19(12):918-931.
50. Yim WW, Mizushima N. Lysosome biology in autophagy. *Cell Discov*. 2020;6(1):6.
51. Forgac M. Vacuolar ATPases: rotary proton pumps in physiology and pathophysiology. *Nat Rev Mol Cell Biol*. 2007;8(11):917-929.
52. Wang R, Wang J, Hassan A, Lee CH, Xie XS, Li X. Molecular basis of V-ATPase inhibition by bafilomycin A1. *Nat Commun*. 2021;12(1):1782.
53. Song SB, Hwang ES. High levels of ROS impair lysosomal acidity and autophagy flux in glucose-deprived fibroblasts by activating ATM and Erk pathways. *Biomolecules*. 2020;10(5):761.
54. Chen Y, Yang Z, Wang S, *et al.* Boosting ROS-mediated lysosomal membrane permeabilization for cancer ferroptosis therapy. *Adv Healthc Mater*. 2023;12(6):e2202150.
55. Norgard MO, Lund PM, Kalisi N, *et al.* Mitochondrial reactive oxygen species modify extracellular vesicles secretion rate. *FASEB Bioadv*. 2023;5(9):355-366.
56. Hedlund M, Nagaeva O, Kargl D, Baranov V, Mincheva-Nilsson L. Thermal- and oxidative stress causes enhanced release of NKG2D ligand-bearing immunosuppressive exosomes in leukemia/lymphoma T and B cells. *PLoS One*. 2011;6(2):e16899.
57. Stepien KM, Roncaroli F, Turton N, *et al.* Mechanisms of mitochondrial dysfunction in lysosomal storage disorders. A review. *J Clin Med*. 2020;9(8):2596.
58. Dan Dunn J, Alvarez LA, Zhang X, Soldati T. Reactive oxygen species and mitochondria: a nexus of cellular homeostasis. *Redox Biol*. 2015;6:472-485.
59. Zeeshan HM, Lee GH, Kim HR, HJ C. Endoplasmic reticulum stress and associated ROS. *Int J Mol Sci*. 2016;17(3):327.
60. Demers-Lamarche J, Guillebaud G, Tlili M, *et al.* Loss of mitochondrial function impairs lysosomes. *J Biol Chem*. 2016;291(19):10263-10276.
61. Heid ME, Keyel PA, Kamga C, Shiva S, Watkins SC, Salter RD. Mitochondrial reactive oxygen species induces NLRP3-dependent lysosomal damage and inflammasome activation. *J Immunol*. 2013;191(10):5230-5238.
62. Weinberg SE, Sena LA, Chandel NS. Mitochondria in the regulation of innate and adaptive immunity. *Immunity*. 2015;42(3):406-417.
63. Neikirk K, Marshall AG, Kula B, Smith N, LeBlanc S, Hinton A. MitoTracker: a useful tool in need of better alternatives. *Eur J Cell Biol*. 2023;102(4):151371.
64. Shelbayeh A, Arroum O, Morris T, Busch S, B K. PGC-1alpha is a master regulator of mitochondrial lifecycle and ROS stress response. *Antioxidants (Basel)*. 2023;12(5):1075.
65. LeBleu VS, O'Connell JT, Gonzalez Herrera KN, *et al.* PGC-1alpha mediates mitochondrial biogenesis and oxidative phosphorylation in cancer cells to promote metastasis. *Nat Cell Biol*. 2014;16(10):992-1003.
66. Hu S, Feng J, Wang M, *et al.* Nrf1 is an indispensable redox-determining factor for mitochondrial homeostasis by integrating multi-hierarchical regulatory networks. *Redox Biol*. 2022;57:102470.
67. Chen T, Li D, Wang Y, *et al.* Loss of NDUFS1 promotes gastric cancer progression by activating the mitochondrial ROS-HIF1alpha-FBLN5 signaling pathway. *Br J Cancer*. 2023;129(8):1261-1273.
68. Ravi S, Pena KA, Chu CT, Kiselyov K. Biphasic regulation of lysosomal exocytosis by oxidative stress. *Cell Calcium*. 2016;60(5):356-362.
69. Bonora M, Giorgi C, Pinton P. Molecular mechanisms and consequences of mitochondrial permeability transition. *Nat Rev Mol Cell Biol*. 2022;23(4):266-285.
70. You S, Barkalifa R, Chaney EJ, *et al.* Label-free visualization and characterization of extracellular vesicles in breast cancer. *Proc Natl Acad Sci U S A*. 2019;116(48):24012-24018.
71. Hu Q, Ren J, Li G, *et al.* The mitochondrially targeted antioxidant MitoQ protects the intestinal barrier by ameliorating

- mitochondrial DNA damage via the nrf2/ARE signaling pathway. *Cell Death Dis.* 2018;9(3):403.
72. Kelso GF, Porteous CM, Coulter CV, *et al.* Selective targeting of a redox-active ubiquinone to mitochondria within cells: antioxidant and antiapoptotic properties. *J Biol Chem.* 2001;276(7):4588-4596.
 73. Peinado H, Aleckovic M, Lavotshkin S, *et al.* Melanoma exosomes educate bone marrow progenitor cells toward a pro-metastatic phenotype through MET. *Nat Med.* 2012;18(6):883-891.
 74. Qian L, Yang X, Li S, *et al.* Reduced O-GlcNAcylation of SNAP-23 promotes cisplatin resistance by inducing exosome secretion in ovarian cancer. *Cell Death Discov.* 2021;7(1):112.
 75. Chacko BK, Srivastava A, Johnson MS, *et al.* Mitochondria-targeted ubiquinone (MitoQ) decreases ethanol-dependent micro and macro hepatosteatosis. *Hepatology.* 2011;54(1):153-163.
 76. Dashdorj A, Jyothi KR, Lim S, *et al.* Mitochondria-targeted antioxidant MitoQ ameliorates experimental mouse colitis by suppressing NLRP3 inflammasome-mediated inflammatory cytokines. *BMC Med.* 2013;11(1):178.
 77. Capeloa T, Krzystyniak J, d'Hose D, *et al.* Mitoq inhibits human breast cancer cell migration, invasion and clonogenicity. *Cancers (Basel).* 2022;14(6):1516.
 78. Capeloa T, Van de Velde JA, d'Hose D, *et al.* Inhibition of mitochondrial redox signaling with MitoQ prevents metastasis of human pancreatic cancer in mice. *Cancers (Basel).* 2022;14(19):4918.
 79. Wang X, Luo G, Zhang K, *et al.* Hypoxic tumor-derived Exosomal miR-301a mediates M2 macrophage Polarization via PTEN/PI3Kgamma to promote pancreatic cancer metastasis. *Cancer Res.* 2018;78(16):4586-4598.
 80. Ding J, Xu Z, Zhang Y, *et al.* Exosome-mediated miR-222 transferring: an insight into NF-kappaB-mediated breast cancer metastasis. *Exp Cell Res.* 2018;369(1):129-138.
 81. Leal AC, Mizurini DM, Gomes T, *et al.* Tumor-derived exosomes induce the formation of neutrophil extracellular traps: implications for the establishment of cancer-associated thrombosis. *Sci Rep.* 2017;7(1):6438.
 82. Zhou J, Li X, Wu X, *et al.* Exosomes released from tumor-associated macrophages transfer miRNAs that induce a treg/Th17 cell imbalance in epithelial ovarian cancer. *Cancer Immunol Res.* 2018;6(12):1578-1592.
 83. Seo N, Akiyoshi K, Shiku H. Exosome-mediated regulation of tumor immunology. *Cancer Sci.* 2018;109(10):2998-3004.
 84. Yin Z, Ma T, Huang B, *et al.* Macrophage-derived exosomal microRNA-501-3p promotes progression of pancreatic ductal adenocarcinoma through the TGFBR3-mediated TGF-beta signaling pathway. *J Exp Clin Cancer Res.* 2019;38(1):310.
 85. Yang M, Chen J, Su F, *et al.* Microvesicles secreted by macrophages shuttle invasion-potentiating microRNAs into breast cancer cells. *Mol Cancer.* 2011;10(1):117.
 86. Walker ND, Elias M, Guiro K, *et al.* Exosomes from differentially activated macrophages influence dormancy or resurgence of breast cancer cells within bone marrow stroma. *Cell Death Dis.* 2019;10(2):59.
 87. Citrin KM, Fernandez-Hernando C, Suarez Y. MicroRNA regulation of cholesterol metabolism. *Ann N Y Acad Sci.* 2021;1495(1):55-77.
 88. Record M, Attia M, Carayon K, *et al.* Targeting the liver X receptor with dendrogenin A differentiates tumour cells to secrete immunogenic exosome-enriched vesicles. *J Extracell Vesicles.* 2022;11(4):e12211.